Geological Society of America Bulletin

Neogene block rotation in central Iran: Evidence from paleomagnetic data

Massimo Mattei, Francesca Cifelli, Giovanni Muttoni, Andrea Zanchi, Fabrizio Berra, Fathollah Mossavvari and Safar Ali Eshraghi

Geological Society of America Bulletin published online 13 January 2012;
doi: 10.1130/B30479.1

Geological Society of America Bulletin, published online on 13 January 2012 as doi:10.1130/B30479.1

Neogene block rotation in central Iran: Evidence from paleomagnetic data

Massimo Mattei[1], Francesca Cifelli[1,†], Giovanni Muttoni[2], Andrea Zanchi[3], Fabrizio Berra[3], Fathollah Mossavvari[4], and Safar Ali Eshraghi[4]

[1]*Dipartimento di Scienze Geologiche, Università Roma TRE, Largo San Leonardo Murialdo 1, 00146 Roma, Italy*
[2]*Dipartimento di Scienze della Terra, Università di Milano, Via Mangiagalli 34, 20133 Milano, Italy*
[3]*Dipartimento Scienze Geologiche e Geotecnologie, Università di Milano-Bicocca, Piazza della Scienza 4, 20126 Milano, Italy*
[4]*Geological Survey of Iran, Azadi Square, Meraj Avenue, 13185-1494, Tehran, Iran*

ABSTRACT

Paleomagnetic results from Oligocene–Miocene sedimentary units in central Iran are used to reconstruct the history of Neogene tectonic deformation of this region. Paleomagnetic data show that in central Iran, crustal blocks bounded by sets of strike-slip faults are rotated to accommodate NNE-SSW shortening related to Arabia-Eurasia convergence. Counterclockwise rotations of 20°–35° have been measured in the Tabas and Anarak areas, south of the Great Kavir fault, characterized by the presence of N-S to NNW-SSE right-lateral strike-slip faults. Conversely, in the Great Kavir and Torud areas, where ENE-WSW left-lateral strike-slip faults have been recognized, paleomagnetic results are less conclusive because the small amount of measured clockwise rotation shows a statistical uncertainty, which also includes the possibility of no rotation. Some of these faults have been active during the Quaternary up to present day, suggesting the possibility that block rotation is still occurring in central Iran.

INTRODUCTION

Shortening related to Arabia-Eurasia convergence in the Cenozoic has been—and is at present being—taken up mainly by displacements in the Zagros, Alborz, and Kopeh-Dag fold-and-thrust belts of Iran, whereas the intervening, fault-bounded crustal blocks of central Iran (Yazd, Tabas, and Lut blocks) show little internal deformation (Fig. 1A).

This deformation pattern is consistent with the distribution of seismicity and recent global positioning system (GPS) studies, which show that at longitude 55°E, the ~22 ± 2 mm/yr of Arabia-Eurasia convergence is mostly accommodated in the Zagros fold-and-thrust belt (~9 ± 2 mm/yr) and in the Alborz and Kopeh-Dagh Mountains (~8 ± 2 mm/yr), whereas only ~4 ± 2 mm/yr is taken up in central Iran (Vernant et al., 2004).

Central Iran is separated from the Alborz belt by NE-SW left-lateral strike-slip and thrust faults (e.g., the Great Kavir fault; Fig. 1B), whereas N-S right-lateral strike-slip faults define the boundary between the Tabas and Lut blocks within central Iran (e.g., the Nayband fault; Fig. 1B), and E-W left-lateral strike-slip and thrust faults prevail along the northern boundary of the Lut block (Jackson and McKenzie, 1984; Jackson and McKenzie, 1988; Jackson et al., 1995; Walker and Jackson, 2004) (Fig. 1A). Despite the occurrence of large strike-slip faults, GPS data and distribution of seismicity show that, as opposed to the pattern occurring along the Iranian western border, where Anatolian faults are first-order examples of lateral transport of continental crust from a collision zone, there is no net transport of Iranian crust eastward with respect to stable Eurasia (Vernant et al., 2004). This difference is probably due to different boundary conditions between western and eastern Iran, the latter of which is characterized by the absence of a "free surface," which could allow the eastern Iranian crust to escape laterally (Allen et al., 2006).

Based on structural and seismological data, it has been proposed that NE-SW left-lateral and N-S right-lateral faults can accommodate the NNE-SSW convergence of Arabia-Eurasia if they are allowed to rotate clockwise (CW) and counterclockwise (CCW), respectively (Freund, 1970; Jackson and McKenzie, 1984; Jackson and McKenzie, 1988; Jackson et al., 1995; Walker and Jackson, 2004; Allen et al., 2011) (Fig. 1C). A rotating-fault deformation model predicts that the intervening fault-bounded rigid blocks should rotate according to the motion on the bounding faults. To test this hypothesis, we applied paleomagnetism, which has been shown to be a powerful tool to gauge the amount and sense of vertical-axis block rotations in different tectonic settings (McKenzie and Jackson, 1983; Ron et al., 1984, 1990; Terres and Luyendyk, 1985; Nur and Ron, 1987; Wells and Hillhouse, 1989; Mattei et al., 2004). In the recent years, paleomagnetic research in Iran has mainly been focused on the reconstruction of the late Paleozoic–early Mesozoic northward drift of the Cimmerian blocks (Besse et al., 1998; Muttoni et al., 2009a, 2009b). Conversely, few paleomagnetic data are available from Jurassic to Cenozoic units (Wensink, 1982; Bina et al., 1986; Soffel et al., 1996; Ballato et al., 2008), leaving the post-Cimmerian history of central Iran poorly constrained.

Paleomagnetic sampling was carried out on Oligocene–Miocene sediments from different areas of central Iran, an area dominated by right-lateral and left-lateral strike-slip fault activity (Fig. 1B). Our results show that rotation of fault-bounded crustal blocks may be considered a valuable mechanism to accommodate some of the crustal shortening in central Iran due to Arabia-Eurasia convergence.

OLIGOCENE–MIOCENE STRATIGRAPHY OF CENTRAL IRAN

The Oligocene–Miocene stratigraphy in central Iran is characterized by three main units that unconformably overlie Cretaceous and Jurassic sedimentary and metasedimentary rocks. These are the continental red beds of the Lower Red Formation (Oligocene), the marine succession of the Qom Formation (late Oligocene–early Miocene), and the continental red beds of the Upper Red Formation (early–late Miocene) (Gansser, 1955; Morley et al., 2009; Reuter et al., 2009).

The Lower Red Formation consists of a 300–1000-m-thick succession of shales, siltstones, gypsum-bearing marls, sandstones, conglomerates, and evaporites (Gansser, 1955) resting unconformably above well-dated Upper

†E-mail: cifelli@uniroma3.it

 doi: 10.1130/B30479.1; 8 figures; 2 tables.

Geological Society of America Bulletin, published online on 13 January 2012 as doi:10.1130/B30479.1

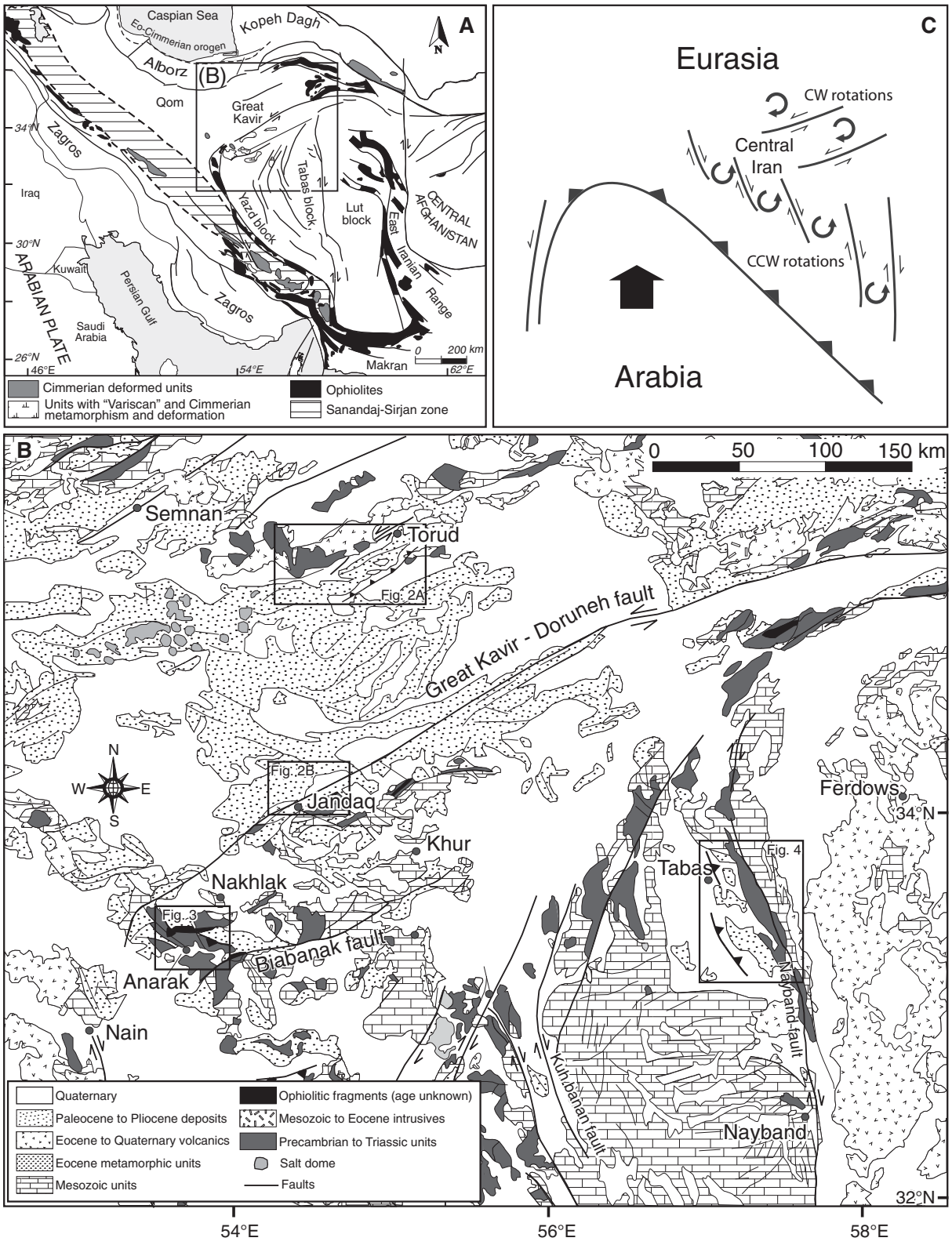

Figure 1. (A) Tectonic scheme of Arabia-Eurasia convergence in the Iranian region. (B) Simplified geological map showing the main tectonic domains in central Iran. Locations of Figures 2, 3, and 4 are also reported (modified from Zanchi et al., 2009). (C) Kinematic sketch showing how the indentation of the Arabian plate northward may be achieved on NNW-SSE right-lateral (by counterclockwise [CCW] rotations) and NE-SW left-lateral strike-slip faults (by clockwise [CW] rotations) (from Allen et al., 2011).

Geological Society of America Bulletin, published online on 13 January 2012 as doi:10.1130/B30479.1

Eocene sediments and underlying the Lower Oligocene–Lower Miocene marine limestones of the Qom Formation (Bozorgnia, 1966; Reuter et al., 2009).

The Qom Formation includes marine limestones, marls, shales, sandstones, and minor gypsum layers (Gansser, 1955; Jackson et al., 1990) with late Rupelian to mid-Burdigalian (early Oligocene–early Miocene) nannofossils (Reuter et al., 2009). In the western part of the depositional area, the Qom Formation is thicker and shows a major temporal range, whereas it progressively decreases eastward in the Great Kavir Basin, where transgressive marine sedimentation occurred only in early Miocene times. Farther eastward, in eastern Iran, the Lower Miocene marine sediments pinch out, and the Upper Red Formation unconformably overlies the Lower Red Formation (Jackson et al., 1990).

Most of the gently folded red beds exposed in the Great Kavir Basin belong to the Upper Red Formation, which is subdivided into three members. The ~700-m-thick lower member consists of gypsum- and salt-rich mudstones and sandstones. Above that, the middle member consists of a 2000–3000-m-thick alternation of gypsiferous mudstones and siltstones. The upper member is >1000 m thick and consists of fine-grained sandstones with thin intercalations of conglomerates overlain by cyclic alternations of saline mudstones and gypsum layers followed in the upper part by salt beds. Recent magnetostratigraphic data from sections located to the south of the Alborz Mountains indicate that deposition of this unit occurred between 17.5 and 7.5 Ma (late Burdigalian–late Tortonian; Ballato et al., 2008).

In the Alborz area, the Upper Red Formation is overlain by the Hezardarreh and Kahrizak Formations, which are coarse-grained siliciclastic alluvial-fan deposits. In the Great Kavir area, thick stacks of Eocene–Oligocene and Miocene salt layers favored the development of salt diapirs, which punched through folded Miocene sedimentary units (Gansser, 1955; Jackson et al., 1990). The presence of salt controlled the deformation style of compressive structures of the Great Kavir (Jackson et al., 1990).

GEOLOGY OF THE SAMPLING SITES

We investigated four areas (Fig. 1B) that are representative of the different orientation and kinematics of the main strike-slip fault systems of central Iran. The Tabas and Anarak sampling areas are located south of the Great Kavir fault, where regional NNW-SSE to N-S right-lateral strike-slip and NW-SE thrust faults prevail, whereas the Torud and Jandaq sampling areas are located in the Great Kavir Basin along ENE-WSW left-lateral strike-slip and thrust faults (Fig. 1). Four to 16 cores with 2.5 cm diameter were drilled at each site using a gasoline-powered drill and oriented in situ with a magnetic compass corrected to account for a local ~4° magnetic declination. Cores were taken from different stratigraphic levels in order to average secular variation of the geomagnetic field and to check for the occurrence of polarity reversals.

Torud

The Torud area (Fig. 2A) is bounded to the north by a Jurassic metamorphic complex (Torud Range), which forms the northern boundary of the Great Kavir region (Alevi and Houshmand-Zadeh, 1976). This area exhibits a simple pattern of gentle ENE-WSW–trending anticlines and synclines, affecting the Miocene Upper Red Formation. In the western part of the area, the development of these structures is controlled by the presence of salt domes (Jackson et al., 1990).

Active tectonics have been recently documented in the Torud area by a catastrophic earthquake (12 February 1953, Ms = 6.4). Field observations (Abdalian, 1953; Tchalenko, 1974) indicate that the Torud earthquake was associated with fault movement along an ENE-trending fault zone. The kinematics of this fault zone are controversial, and both left-lateral and thrust movements have been suggested (Shirokova, 1962; Ambraseys and Moinfar, 1977; Jackson and McKenzie, 1984; Walker and Jackson, 2004; Eshraghi and Jalali, 2006).

In the Torud area, we sampled six sites (IR40–IR45) along the southern margin of a WNW-dipping homocline of Miocene units that is characterized by parasitic folds in its southern part. Further sampling was carried out in the ENE-WSW North Moalleman anticline, which extends along the northeastern margin of the Great Kavir just to the southwest of the Torud uplift. The anticline folds the Upper Red Formation, and it is intersected in its western part by a salt diapir (Jackson et al., 1990). We sampled two sites (IR46, IR47) in the red marls and silty marls of the Upper Red Formation along the southern flank of the anticline, and two other sites (IR48, IR49) in the red marls of the Upper Red Formation along the northern flank of the anticline (Fig. 2A).

Jandaq

The Jandaq area (Fig. 2B) is located along the ENE-WSW left-lateral Great Kavir fault (Fig. 1). In the area between Jandaq and Anarak to the south of the Great Kavir fault, units pertaining to a late Paleozoic–Triassic active margin have been recently recognized (Bagheri and Stampfli, 2008; Zanchi et al., 2009). These findings suggest that the present-day Great Kavir fault may be an ancestral structure inherited from a late Paleozoic–Triassic tectonic boundary. No recent or historical seismicity is clearly associated with the Great Kavir fault, but morphological evidence of tectonic activity is suggested by the presence of fault scarps in recent alluvial deposits (Walker and Jackson, 2004).

In the Jandaq area, we sampled four sites in the marls and siltstones of the Upper Red Formation (Fig. 2B). Three sites (IR36–IR38) were sampled to the south of the Great Kavir fault along the limbs of an ENE-WSW–trending syncline, whereas site IR39 was sampled to the north of the Great Kavir fault along the SSE-dipping limb of another ENE-WSW–trending fold.

Anarak

The Anarak area (Fig. 3) is located in western central Iran, 40 km to the south of the Great Kavir fault (Fig. 1). The main tectonic element of the area is the Anarak metamorphic complex, which consists of metapelites, metabasites, and marbles associated with slivers of ultramafic rocks (Sharkovski et al., 1984), and which has been interpreted as an accretionary wedge that formed between the late Paleozoic and Triassic (Bagheri and Stampfli, 2008; Zanchi et al., 2009). A WNW-ESE–striking thrust fault places rocks of the metamorphic complex on top of a Cenozoic terrigenous succession that crops out to the north in a WNW-ESE–trending fold belt and includes Eocene to Lower Miocene red marls, siltstones, sandstones, and conglomerates of the Sahlab Formation, Lower Red Formation, and Qom Formation (Sharkovski et al., 1984). The orientation of the fault marking the contact between the metamorphic complex and the Cenozoic sequence implies a NE-SW direction of horizontal compression, consistent with the trend of fold axes developed within the Cenozoic sediments. The Cenozoic succession is bound to the north by reverse faults with a WNW-ESE trend and by conjugate strike-slip faults that displace the contact with a granitoid intrusive (Zanchi et al., 2009).

In the Anarak area, one site (IR08) was sampled in the Middle to Upper Eocene siltstones of the Sahlab Formation, and five sites were sampled along a WNW-ESE fold developed in the footwall of the main thrust affecting the Anarak metamorphic complex, and specifically in the Oligocene–Lower Miocene marls and silty marls of the Lower Red Formation (IR09, IR15–IR16) and Qom Formation (IR10–IR11) (Fig. 3).

Geological Society of America Bulletin, published online on 13 January 2012 as doi:10.1130/B30479.1

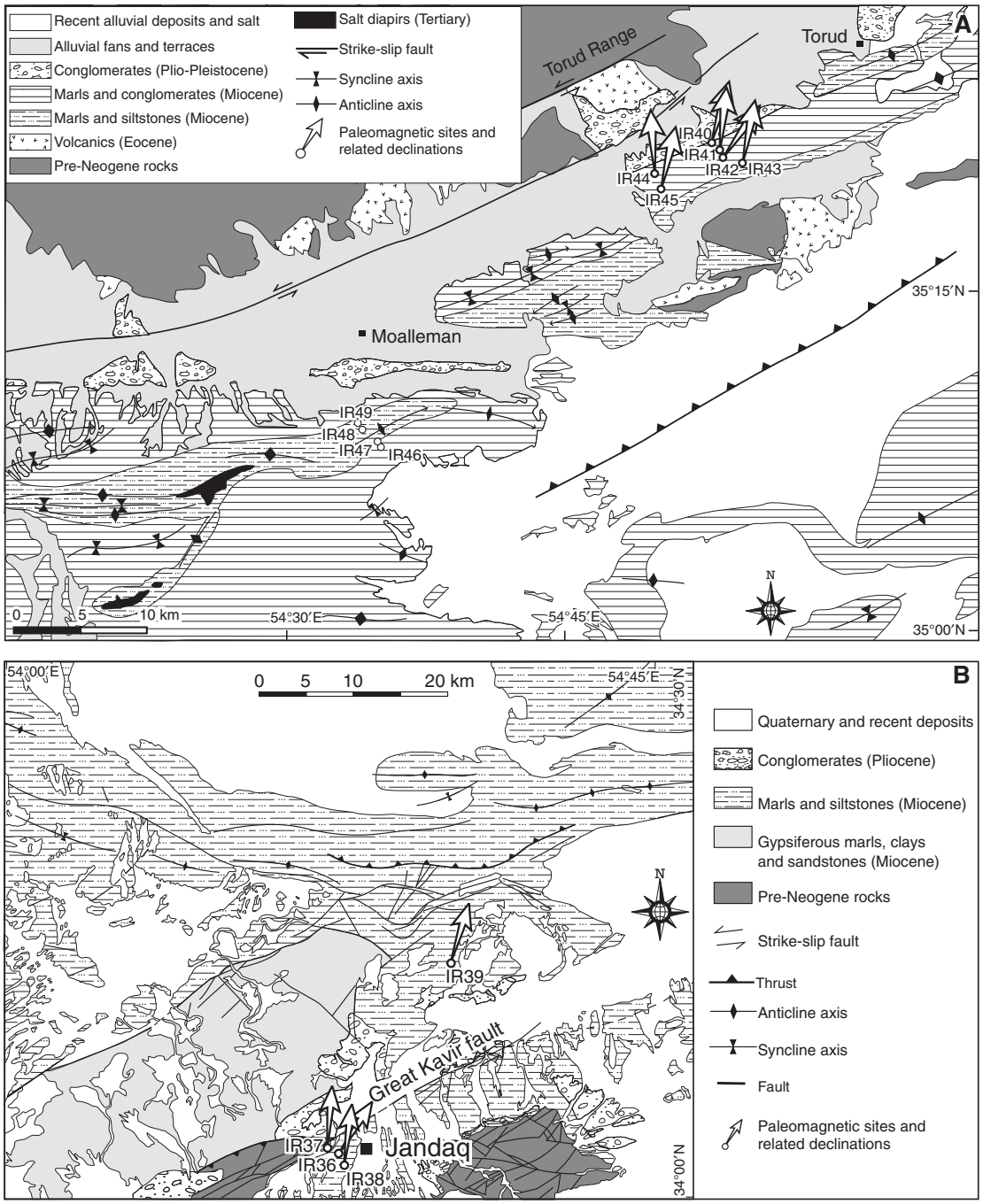

Figure 2. Synthetic structural maps of the sampled zones north of the Great Kavir–Doruneh fault, in the Great Kavir Basin. (A) The Torud and Moalleman region, with main fault and fold systems (modified from Alevi and Houshmand-Zadeh, 1976; Jackson et al., 1990). (B) The Jandaq region (modified from Babakhani et al., 1987). The locations of the paleomagnetic sites and respective paleomagnetic declinations are shown.

Tabas

The Tabas area (Fig. 4) is situated in the northern part of the Tabas block (Fig. 1). The northern part of the Tabas block is characterized by the Tabas Basin (Stöcklin and Nabavi, 1971), which hosts a NNW-SSE–trending fold system developed along the western foothills of the Shotori Range. The Shotori Range separates the Tabas block from the Lut block to the east (Fig. 4). The transition between the Tabas folds and the Shotori Range is characterized by an abrupt change in elevation (~1000 m) and represents a tectonic boundary that has been active since pre-Paleozoic times, as suggested by large changes in Precambrian and Paleozoic sediment thicknesses occurring across the boundary (Stöcklin et al., 1965; Berberian, 1979a).

Geological Society of America Bulletin, published online on 13 January 2012 as doi:10.1130/B30479.1

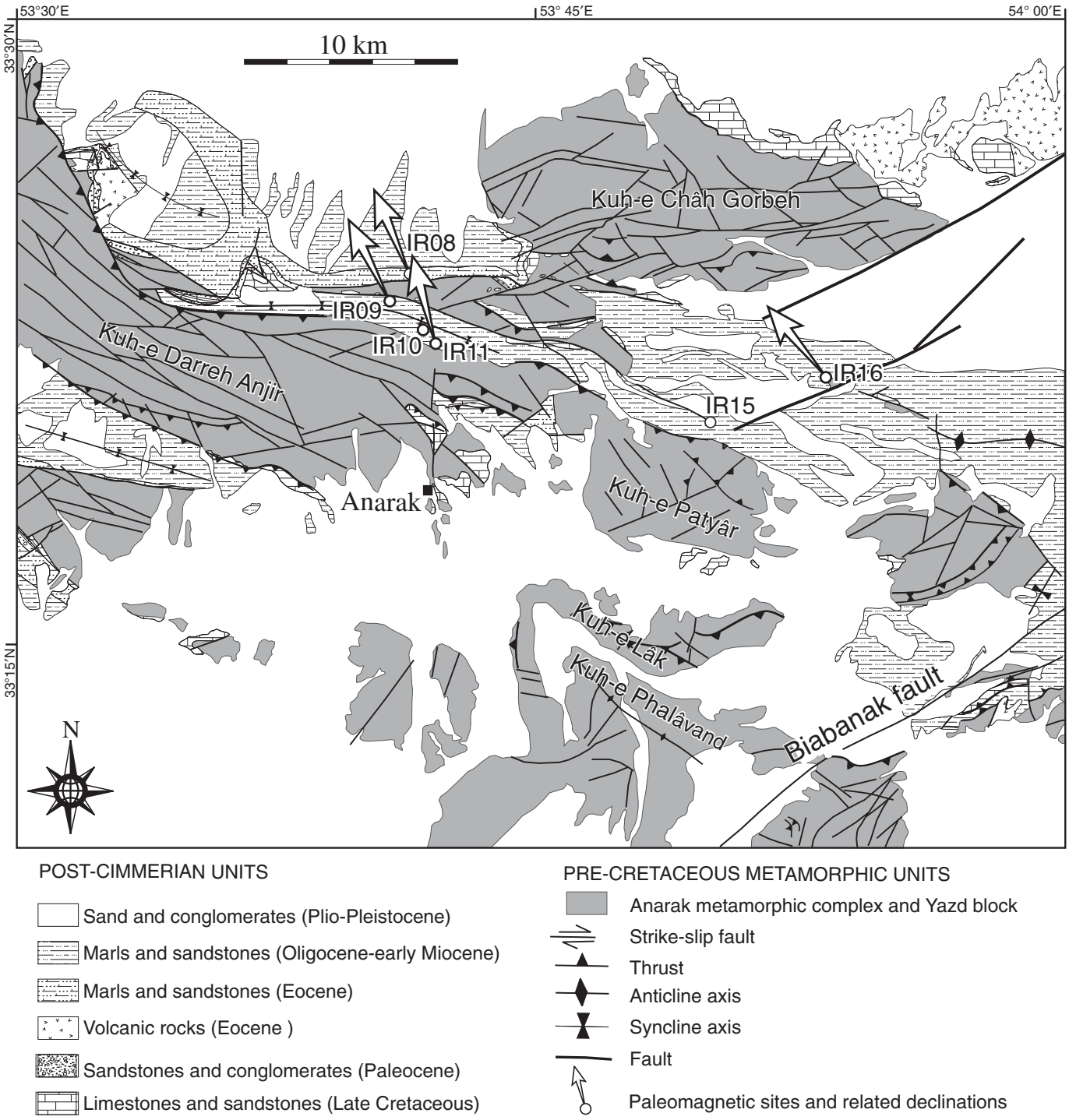

Figure 3. Synthetic structural map of the Anarak region, showing the main fault and fold systems. The locations of the paleomagnetic sites and respective paleomagnetic declinations are indicated (modified from Nabavi and Houshmand-zadeh, 1984).

Neogene sediments in the area consist of red marls, silty marls, and gypsum layers of the Upper Red Formation (Berberian, 1979a), which crop out in the cores of major anticlines, and which are overlain by a thick sequence of fluvial and alluvial-plain conglomerates. In the southern and northern sectors of the Tabas Basin, these Neogene sediments are thin, and the fluvial conglomerates locally lie directly on the pre-Neogene bedrock. Conversely, toward the central and western parts of the basin, the Neogene strata reach a thickness of several hundred meters.

The catastrophic 1978 Tabas earthquake of Ms 7.4 produced a discontinuous series of surface ruptures extending for 85 km in the NNW

Geological Society of America Bulletin, published online on 13 January 2012 as doi:10.1130/B30479.1

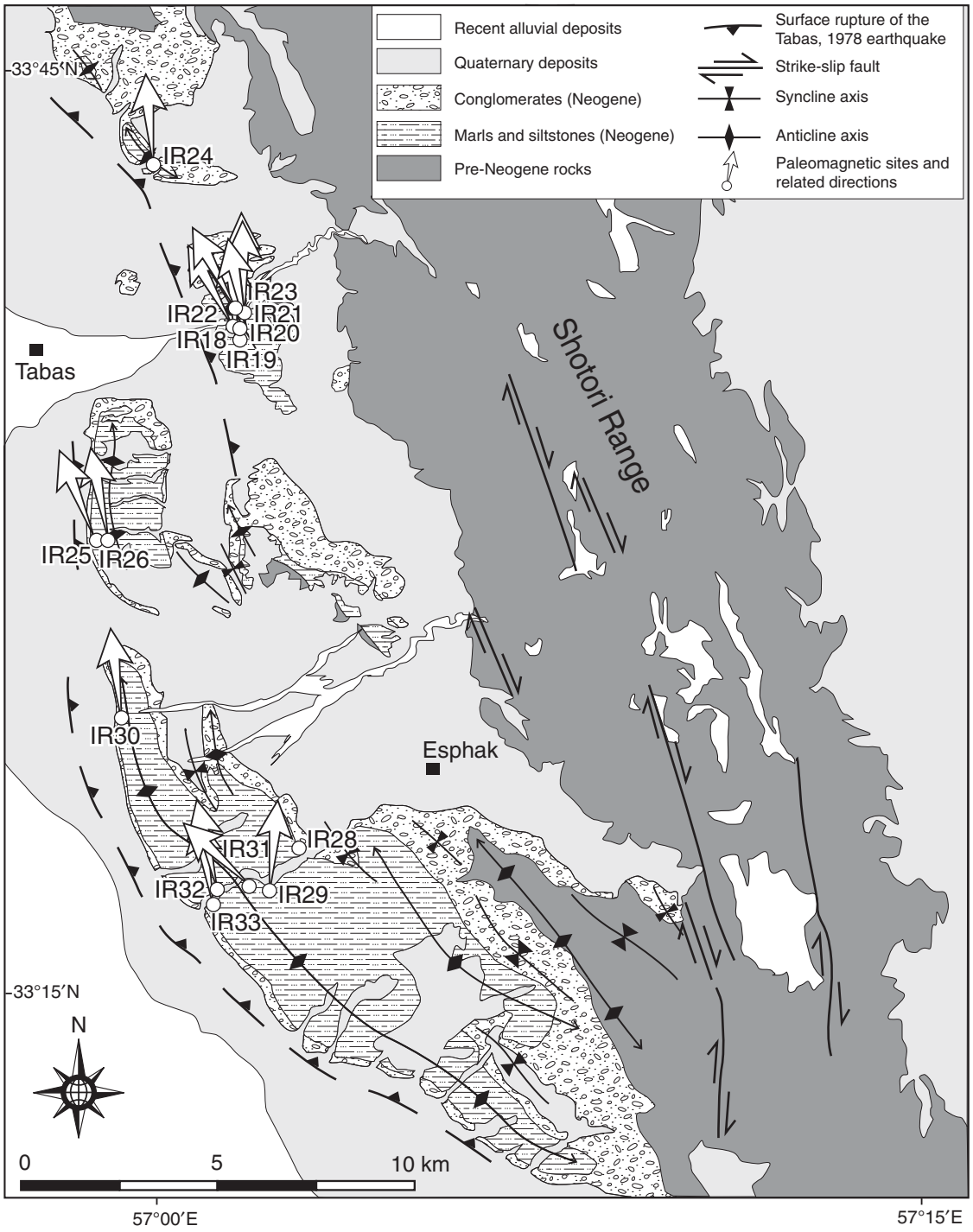

Figure 4. Synthetic structural map of the Tabas region, with the locations of the paleomagnetic sites and relative paleomagnetic declinations (modified from Stöcklin et al., 1965; Stöcklin and Nabavi, 1969; Aghanabati, 1974).

direction. Focal mechanism, aftershock distribution, surface deformation, and faulting concordantly show that the Tabas earthquake occurred along a previously unrecognized NW- to NNW-striking thrust fault with a small component of right-lateral strike slip. Thrust faults, including the one that ruptured during the Tabas earthquake, and related folds placed Neogene and older strata over younger strata to the west, buried below the Tabas depression (Berberian, 1979a, 1979b, 1982; Berberian et al., 1979; Niazi and Kanamori, 1981; Silver and Jordan, 1983; Walker et al., 2003).

In the Tabas fold system, we sampled 15 sites in the Neogene Upper Red Formation (Fig. 4). Seven sites (IR18–IR23) were sampled along a major anticline located east of Tabas village and exposed along the Sardar River. Five sites (IR28–IR29 and IR31–IR33) were sampled

Geological Society of America Bulletin, published online on 13 January 2012 as doi:10.1130/B30479.1

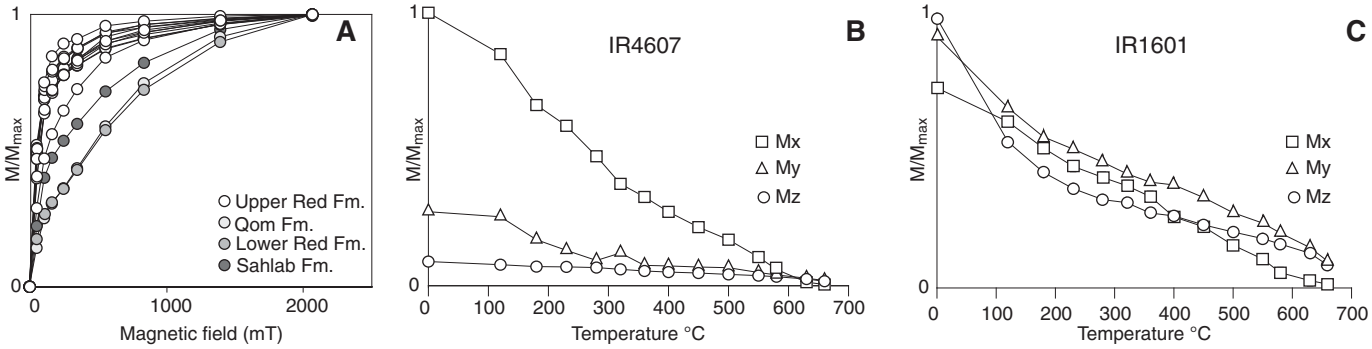

Figure 5. Isothermal remanent magnetization (IRM) acquisition curves (A) and thermal demagnetization of a three-component IRM (Lowrie, 1990) from representative magnetite-rich samples (B) and hematite-rich samples (C). M—magnetization value at each magnetic field step; M_{max}—maximum magnetization; Mx, My, Mz—magnetization along the *x*, *y*, *z* specimen axes, respectively.

along the river incision that cuts the core of the Esphak anticline, 50 km to the south of Tabas village. One more site (IR30) was sampled in the western flank of the same anticline. Finally, one site (IR24) was sampled along the western flank of the Posha fold, in the northern Tabas fold system. Two other sites (IR25, IR26) were sampled along the western limb of the fold located immediately to south of Tabas village.

METHODS AND RESULTS

Isothermal remanent magnetization (IRM) acquisition curves and thermal demagnetization of a three-component IRM were used to investigate magnetic mineralogy on representative specimens from the Sahlab Formation (IR08), Qom Formation (IR10), Lower Red Formation (IR17), and Upper Red Formation (IR20–21, IR24, IR26, IR29, IR33, IR40, IR42–43, IR46–49). The stepwise acquisition of an isothermal remanent magnetization (IRM) was imparted using a pulse magnetizer up to 2.1 T fields. A three-component IRM was imparted at 1.7 T, 0.6 T, and 0.12 T fields along the samples' orthogonal axes and thermally demagnetized according to the procedure of Lowrie (1990). Most of the Upper Red Formation samples neared saturation at 200–300 mT fields, whereas samples from the Sahlab, Lower Red, and Qom Formations did not reach saturation up to 2100 mT, suggesting that in the sampled units, both low- and high-coercivity ferromagnetic minerals are present in different percentages (Fig. 5A). Thermal demagnetization of a three-component IRM confirmed these results and helped to define the nature of the magnetic minerals. The low-coercivity minerals show maximum unblocking temperatures of ~580–620 °C, indicating magnetite and maghemite as main magnetic carriers (Fig. 5B). High-coercivity magnetic phases show a sharp decrease around 100–200 °C followed by maximum unblocking temperatures of ~680 °C, attributed to goethite and hematite, respectively (Fig. 5C).

Samples were demagnetized using a 2G Enterprises dc SQUID (superconducting quantum interference device) cryogenic magnetometer located in a shielded room at the Alpine Laboratory of Paleomagnetism of Peveragno (Italy). The natural remanent magnetization (NRM) of one specimen per core was measured by means of progressive stepwise thermal demagnetization using small temperature increments (80–100 °C up to 300 °C and 30–50 °C above 300 °C) until the NRM decreased below the limit of the instrument sensitivity or random changes of the paleomagnetic directions appeared. After removal of a low-temperature viscous component, most of the samples showed a single component of magnetization, with maximum unblocking temperatures of 610–640 °C for the hematite-bearing samples (Figs. 6A–6C), and of 550–580 °C for magnetite-bearing samples (Figs. 6D–6F). The low-field magnetic susceptibility was measured after each heating step to monitor thermally induced changes in the magnetic mineralogy.

Least-square analysis (Kirschvink, 1980) was applied to determine characteristic remanent magnetization (ChRM) directions. The maximum angular deviation (MAD) of the isolated magnetic components was generally <10°. The site-mean paleomagnetic directions were calculated using Fisher (1953) statistics or the McFadden and McElhinny (1988) method in two sites where remagnetization circles were also observed (Table 1).

Results from 30 sites were used to calculate the overall mean paleomagnetic directions for the different study areas (Fig. 7; Table 1). Mean paleomagnetic rotations were then computed in relation to the fixed Eurasian plate using the coeval European paleopoles from Besse and Courtillot (2002). Rotation values and associated 95% confidence limits (Table 2) were calculated according to the method of Demarest (1983).

Torud

Together, the sites from the Neogene Upper Red Formation of the Torud anticline gave well-grouped site-mean directions, with α_{95} values between 4.5° and 14.5°. Four sites show normal polarity, one site shows reverse polarity, and one site shows normal and reverse polarity from distinct layers. When all the sites are considered together, the reversal test of McFadden and McElhinny (1990) is indeterminate. Site-mean paleomagnetic directions are better grouped after tectonic correction, although the fold test of McFadden (1990) provides an indeterminate result. After tectonic correction, the overall mean ChRM direction of the six sites is declination (Dec.) = 11.4°, inclination (Inc.) = 39.5°, k = 33.5, α_{95} = 11.7° (Table 1; Fig. 7A). However, site IR44 shows a bedding strike rotated ~30° clockwise with respect to the other sites, which is not representative of the general trend of the Torud structure. If we exclude this site from the computation, the mean ChRM direction of the remaining five sites is Dec. = 15.2°, Inc. = 41.3°, k = 41.4, α_{95} = 12.0°. When this mean direction is compared with the 10 Ma Eurasian paleopole of Besse and Courtillot (2002), a clockwise (CW) rotation R = 9.3° (±13.0°) is observed, with a flattening F = 12.0° (±10°) (Table 2).

Four sites were sampled in the two limbs of the Moalleman anticline (Fig. 2A). In most of the samples, we were able to isolate a normal polarity component, which is stable up to 540–580 °C, whereas only three samples show a high-temperature reverse polarity component isolated up to 580 °C (Fig. 7B). The normal polarity components provide well-grouped site-mean directions in three sites, with α_{95} < 15.0°,

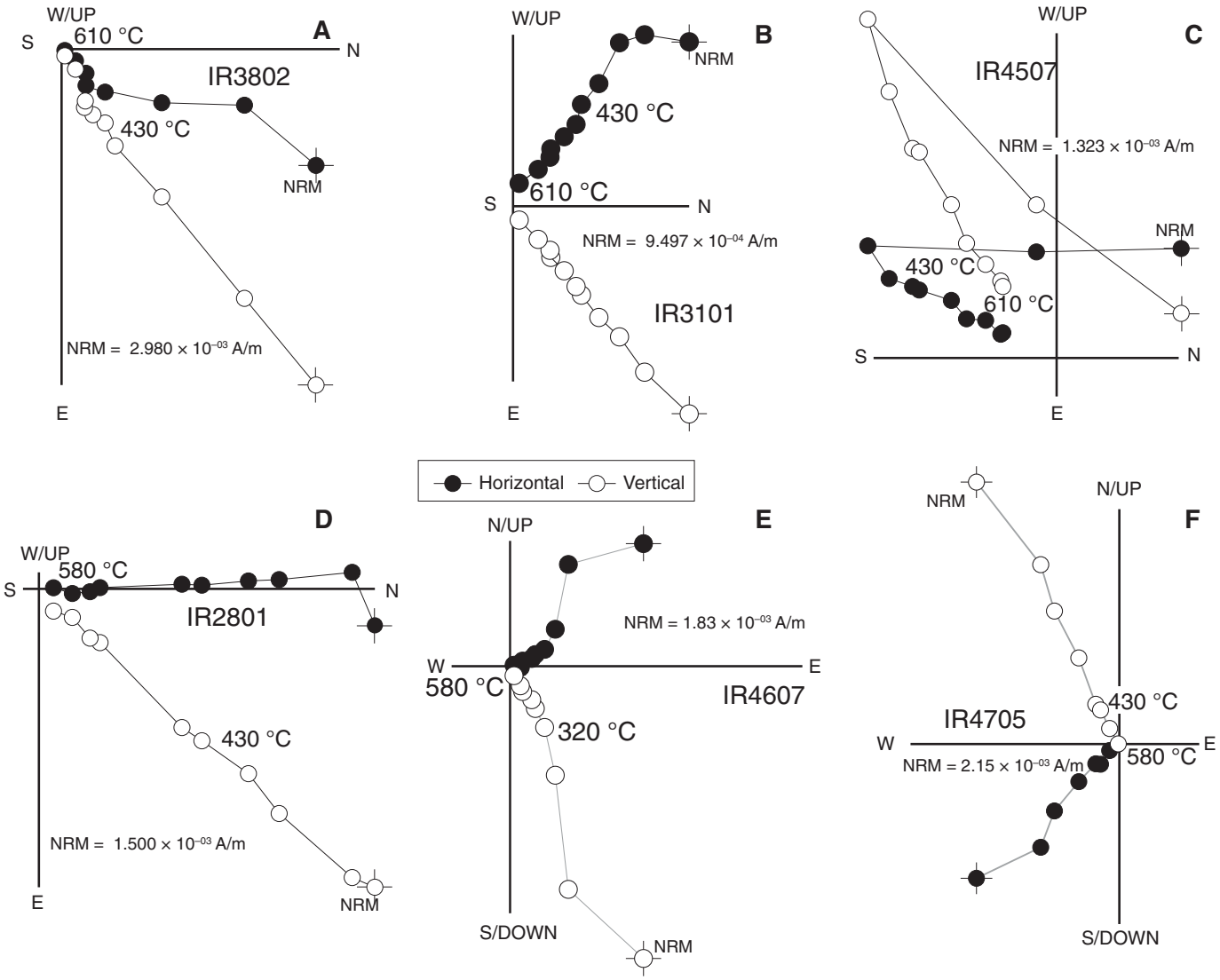

Figure 6. Vector component diagrams for the progressive demagnetization of representative samples. Open and solid symbols represent projections on the vertical and horizontal planes, respectively. N/UP, W/UP, E, and S/DOWN indicate horizontal (north, south, west, and east) and vertical (up and down) projections combined into a single vector component diagram. NRM—natural remanent magnetization.

whereas in one site (IR49), these components yield a more dispersed site-mean direction (α_{95} = 42.9°). When these sites are considered together, they provide an overall mean direction that is better grouped before tectonic correction (Dec. = 15.8°, Inc. = 50.2°, k = 44.3, α_{95} = 14.1°) than after tectonic correction (Dec. = 17.2°, Inc. = 46.8°, k = 6.7, α_{95} = 38.3°) (Table 1). This overall mean direction in geographic coordinates (before tectonic correction) is very close to the present-day geocentric axial dipole (GAD) field for central Iran (Fig. 7B). Based on these observations, we suggest that sites from the North Moalleman anticline have been subjected to a postfolding pervasive remagnetization overprint of normal polarity. A high-temperature magnetic component of reverse polarity, regarded as primary (syndepositional) in age, was successfully isolated in only three samples. This magnetic component is rotated relative to the expected result both before tectonic correction (Dec. = 222.7°, Inc. = –29.9°) and after tectonic correction (Dec. = 222.4°, Inc. = –30.1°), suggesting a possible CW rotation of the North Moalleman Lower Red Formation.

Jandaq

In the Jandaq area, four sites gave paleomagnetic components of normal polarity, with α_{95} values between 8.3° and 10.8°. The overall mean paleomagnetic direction of the four sites is better grouped after tectonic correction (Dec. = 14.2°, Inc. = 43.8°, k = 44.6, α_{95} = 13.9°) than before (Dec. = 6.1°, Inc. = 45.0°, k = 13.6, α_{95} = 25.8°) (Table 1; Fig. 7C). The fold test of McFadden (1990) is indeterminate, with a maximum k at 65% unfolding. When compared with the direction expected from the coeval (10 Ma) Eurasian paleopole, a CW rotation R = 8.3° (±15.4°) was calculated (F = 8.8° ± 11.1°) (Table 2).

Anarak

In the Anarak area, reliable results were obtained from four (out of a total of six) sites (IR08, IR09, IR11, and IR16). At site IR10, samples showed an unstable behavior during demagneti-

Geological Society of America Bulletin, published online on 13 January 2012 as doi:10.1130/B30479.1

TABLE 1. PALEOMAGNETIC DIRECTIONS FROM CENTRAL IRAN

		Location						BTC				ATC			
Area	Site	Lat (°N)	Long (°E)	Fm	Lithology	n1, n2/N	S_0	D (°)	I (°)	K (°)	α_{95} (°)	D (°)	I (°)	K (°)	α_{95} (°)
Anarak	IR08	33°23′47.9″	53°41′29.2″	SF	Siltstones	12,0/12	352,76	230.2	74.1	76.6	5.0	337.5	21.9	76.6	5.0
	IR09	33°23′09.3″	53°41′15.0″	LRF	Silty marls	5,0/5	214,87	149.1	26.0	18.6	18.5	153.4	–21.0	18.6	18.5
	IR11	33°22′14.0″	53°41′59.6″	QF	Marls	8,0/8	209,49	2.6	9.4	52	7.8	345.1	50.7	52.0	7.8
	IR15*	33°20′15.2″	53°49′50.9″	LRF	Marls	13,0/13	208,77	205.0	48.3	25.0	8.5	222	13	25.0	8.5
	IR16	33°21′22.0″	53°53′24.1″	LRF	Silty marls	16,0/16	82,15	315.3	16.6	23.8	7.7	320.3	25.1	23.8	7.7
	Mean (4 sites)							**332.3**	**66.3**	**1.5**	**47.1**	**333.2**	**29.9**	**24.1**	**19.1**
Tabas	IR18	33°37′32.2″	57°02′15.5″	URF	Marls	7,0/7	218,40	343.0	9.2	79.5	6.8	330.3	29.1	79.5	6.8
	IR19	33°36′26.1″	57°03′12.6″	URF	Silty marls	14,0/14	60,16	167.7	–31.5	106.7	3.9	175.8	–25.5	106.7	3.9
	IR20	33°36′55.1″	57°03′30.5″	URF	Marls	10,0/10	230,16	181.0	–31.7	50.6	6.9	171.4	–41.2	50.6	6.9
	IR21	33°36′44.6″	57°03′16.5″	URF	Marls	10,0/10	70,25	328.6	51.7	41.4	7.6	360.0	49.7	41.4	6.4
	IR22	33°36′31.7″	57°02′43.8″	URF	Marls	14,0/14	237,66°	17.8	18.1	60.8	5.1	331.2	53.0	60.8	5.1
	IR23	33°36′39.7″	57°03′12.1″	URF	Silty marls	10,0/10	59,20	157.1	–48.7	82.6	5.3	176.8	–42.4	82.6	5.3
	IR24	33°42′53.0″	56°59′03.5″	URF	Silty marls	12,0/12	30,27	136.3	–67.4	58.8	5.7	174.4	–50.7	58.8	5.7
	IR25	33°29′52.4″	56°58′07.8″	URF	Silty marls	5,0/5	251,15	188.5	–53.0	36.6	12.8	167.6	–57.5	36.6	12.8
	IR26	33°29′42.5″	56°57′35.1″	URF	Silty marls	10,2/12	244,59	21.6	21.8	37.2	7.2	337.2	51.2	37.2	7.2
Esphak	IR28*	33°19′46.5″	57°05′54.2″	URF	Marls	5,0/5	30,18	1.6	34.1	46.8	9.9	5.7	21.3	46.8	9.9
	IR29	33°19′12.0″	57°05′32″	URF	Silty marls	13,0/13	47,57	264.3	53.1	73.9	4.9	5.5	57.0	73.9	4.9
	IR30	33°21′58.9″	56°58′33.6″	URF	Silty marls	6,0/6	262,26	18.6	41.7	65.9	8.3	352.8	48.1	65.9	8.3
	IR31	33°18′57.5″	57°03′33.8″	URF	Silty marls	9,0/9	Horiz.	313.4	34.1	46.8	9.9	313.4	34.1	46.8	9.9
	IR32	33°19′01.8″	57°02′53.1″	URF	Silty marls	4,0/4	255,18	7.3	46.1	205.1	6.4	347.5	50.0	205.1	6.4
	IR33	33°18′51.0″	57°02′42.8″	URF	Siltstones	6,0/6	243,35	192.1	–25.8	109.2	6.4	170.1	–43.0	109.2	6.4
	Mean (14 sites)							**352.2**	**41.9**	**8.48**	**14.5**	**346.1**	**46.1**	**33.26**	**7.0**
Jandaq	IR36	34°02′32.5″	54°23′46.3″	URF	Marls	7,0/7	135,52	354.9	22.8	38.7	9.8	32.6	52.7	38.7	9.8
	IR37	34°02′52.2″	54°22′55.4″	URF	Marls	8,0/8	37,11	357.1	52.9	36.3	9.3	4.5	44.0	36.3	9.3
	IR38	34°02′06.3″	54°23′39.4″	URF	Marls	9,0/9	335,42	43.9	61.0	39.2	8.3	7.3	32.2	39.2	8.3
	IR39	34°13′26.4″	54°31′22.5″	URF	Siltstones	4,0/4	126,16	4.3	37.8	73.2	10.8	17.1	44.7	73.2	10.8
	Mean (4 sites)							**6.1**	**45.0**	**13.6**	**25.8**	**14.2**	**43.8**	**44.6**	**13.9**
Torud	IR40	35°21′15.7″	54°53′03.8″	URF	Siltstones	8,0/8	345,20	24.7	71.0	15.5	14.5	5.4	53.4	15.5	14.5
	IR41	35°20′48.2″	54°53′42.1″	URF	Marls	0,6/6	330,25	32.0	46.9	24.2	12.5	15.1	31.8	24.2	12.5
	IR42	35°20′29.2″	54°43′58.1″	URF	Marls	8,0/8	340,20°	56.7	49.2	32.4	9.9	33.6	48.2	32.4	9.9
	IR43	35°19′49.4″	54°54′46.2″	URF	Marls	8,0/8	342,56	70.9	65.9	26.8	10.9	10.2	30.3	26.8	10.9
	IR44	35°19′52.1″	54°53′35.1″	URF	Siltstones	6,0/6	15,42	328.7	65.6	65.7	8.3	355.0	29.1	65.7	8.3
	IR45	35°20′08.1″	54°52′33.1″	URF	Marls	9,0/9	335,22	211.5	–56.4	131.6	4.5	192.9	–41.1	131.6	4.5
	Mean (6 sites)							**34.5**	**62.4**	**19.4**	**15.6**	**11.4**	**39.5**	**33.5**	**11.7**
Moalleman	IR46*	35°07′33.3″	54°35′15.4″	URF	Silty marls	5	158,20	21.4	53.9	23.0	16.3	37.2	65.3	23.0	16.3
	IR47*	36°08′00.3″	54°34′55.9″	URF	Marls	6	150,21	10.5	56.7	107.8	6.5	43.4	68.2	107.8	6.5
	IR48*	35°09′21.3″	54°33′11.0″	URF	Marls	11	340,30	358.4	42.6	44.3	6.9	353.9	13.8	44.3	6.9
	IR49*	35°09′46.7″	54°33′00.4″	URF	Marls	4	326,25	33.1	44.5	5.6	42.9	16.2	31.1	5.6	42.9
	Mean (4 sites)*							**15.8**	**50.2**	**44.3**	**14.1**	**17.2**	**46.8**	**6.7**	**38.3**

Notes: Abbreviations: Fm—geological formation (SF—Sahlab Formation, Eocene; LRF—Lower Red Formation, Oligocene; QF—Qom Formation, early Oligocene–early Miocene; URF—Upper Red Formation, early Miocene–late Miocene); n1, n2/N—number of stable directions, number of great circles/total number of stable directions at a site; D°, I°—site mean declinations and inclinations calculated before tectonic correction (BTC) and after tectonic correction (ATC); K—precision parameter; α_{95}—confident limit (statistical parameters after Fisher, 1953); S_0—bedding attitude (azimuth of the dip and dip values). S_0 values with ° symbol were deduced by anisotropy of magnetic susceptibility tensor.

*Sites not considered further in tectonic interpretation.

zation, and we were not able to isolate a ChRM for this site. Site IR15 showed magnetic component directions oriented southward, with positive inclinations that are regarded as of dubious origin, and they have not been considered for further analyses. ChRM component directions from sites IR08, IR11, and IR16 are well grouped with α_{95} values between 5.0° and 7.8°, whereas ChRM components from site IR09 are more dispersed (α_{95} = 18.7°). These components are of normal polarity in sites IR08, IR11, and IR16, and of reverse polarity in site IR09. The reversal test of McFadden and McElhinny (1990) provides an indeterminate result. Site-mean directions are better grouped after tectonic correction than before tectonic correction, and the fold test is positive at 99% level of confidence according to McFadden (1990). After tectonic correction, the overall mean ChRM direction from the Anarak sites is Dec. = 333.2°, Inc. = 29.9°, k = 24.1, α_{95} = 19.1° (Table 1; Fig. 7D). When compared with the direction expected from the 25 Ma Eurasian paleopole of Besse and Courtillot (2002), a CCW rotation of R = 35.0° (±18.0°) is observed (F = 21.4° ± 15.6°) (Table 2).

Tabas

In the Neogene Upper Red Formation of the Tabas fold system, well-defined ChRM component directions were isolated in 14 of 15 sites, all of which display well-grouped site-mean directions (α_{95} < 13°). Site IR28 was excluded from further analyses because it bears normal polarity component directions oriented along the present-day GAD field direction in geographic coordinates and because after tilt correction, its mean direction diverges from the rest of the Tabas sites. Eight sites show normal polarity components, and six sites show reverse polarity components. The reversal test is positive and classified as Rc (γo = 9.7°; γc = 13.0°) according to McFadden and McElhinny (1990). The site-mean paleomagnetic directions are better grouped after tectonic correction than before tectonic correction, and the fold test is positive at 99% level of confidence according to McFadden (1990). After tectonic correction, the overall mean ChRM direction of the 14 sites from the Neogene upper red beds of the Tabas area is Dec. = 346.1°, Inc. = 46.1°, k = 33.26, α_{95} = 7.0° (Table 1; Fig. 7E). When compared with the direction expected from the 10 Ma Eurasian paleopole from Besse and Courtillot (2002), a CCW rotation of R = 19.8° (±8.4°) is observed (F = 5.7° ± 6°) (Table 2).

TECTONIC IMPLICATIONS

Timing of the Remanent Magnetization Acquisition and its Origin

Paleomagnetic results from central Iran show significant differences in the origin of the measured ChRM, which has been demonstrated to be primary (or early diagenetic) in most of

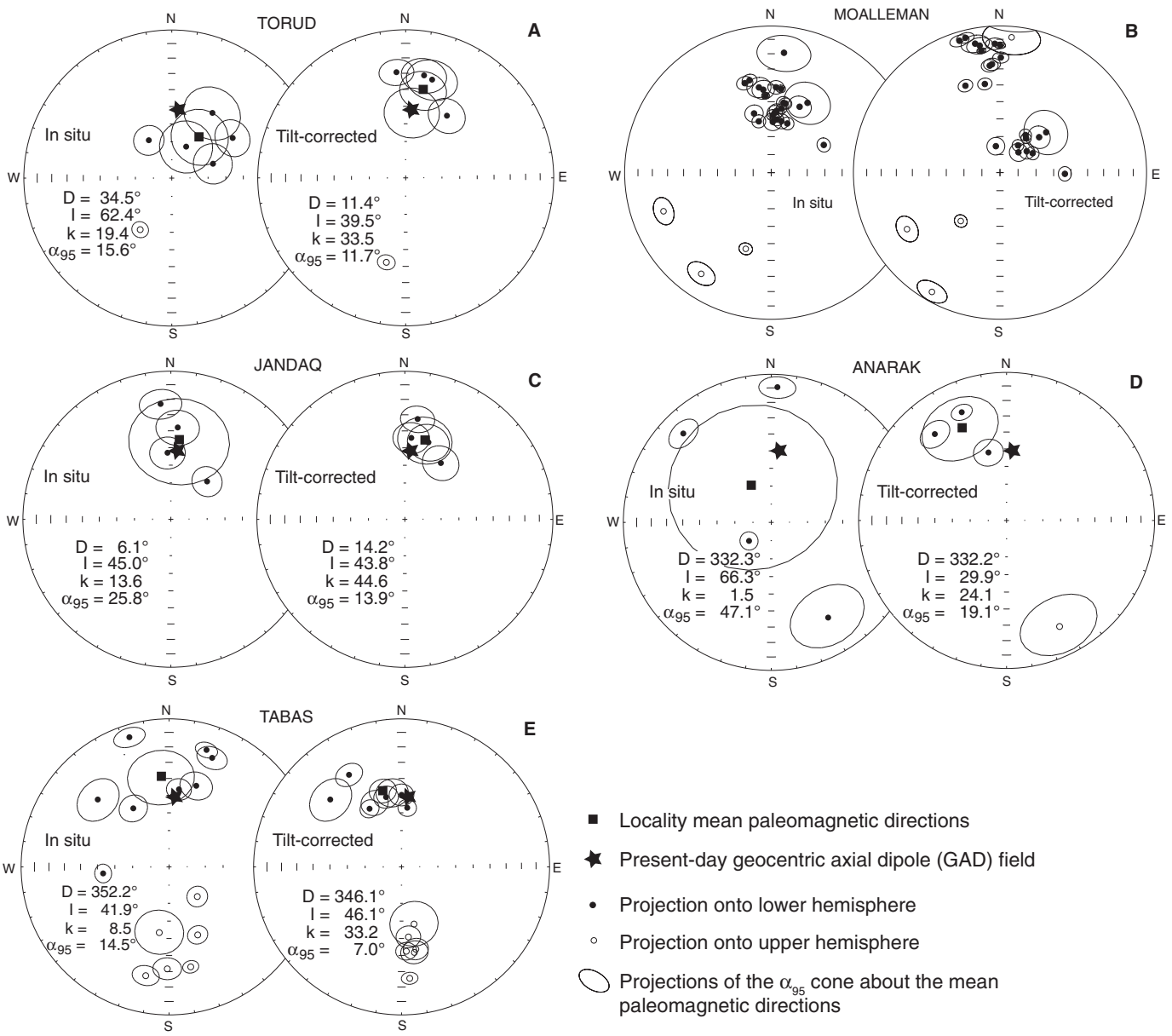

Figure 7. (A) Equal-area projection of the site-mean directions from the Torud area. (B) Equal-area projection of sample characteristic remanent magnetization (ChRM) directions from the Moalleman area (the 95% confidence ellipse for the normal and reverse directions is indicated). Samples with a normal polarity have been affected by a recent magnetic overprint, whereas samples with a reverse polarity show a clockwise (CW) rotated ChRM. (C–E) Equal-area projection of the site-mean directions from the Jandaq, Anarak, and Tabas areas, respectively.

the sampled sites except in the Moalleman area. In particular, sites from Anarak, Tabas, and Torud areas show normal and reverse polarities, and their paleomagnetic mean direction is better grouped after than before tectonic correction (with a positive fold test for the Anarak and Tabas sites). These observations support interpretation of the ChRM in the Anarak, Tabas and Torud sites as a primary (or early diagenetic) magnetization, in agreement with previous paleomagnetic data from the Upper Red Formation of Alborz Mountains (Ballato et al., 2008). A ChRM related to a recent (post-folding) magnetic overprint was detected in the Moalleman area. Here, all four sites show a normal polarity direction, close to the present-day GAD magnetic field, and their mean paleomagnetic direction is better grouped before than after tectonic correction. These paleomagnetic results substantially confirm the multiple origin (detrital and diagenetic) of magnetic particles (mostly hematite), already observed by Amini (2001) on the basis of optical and scanning electron microscope (SEM) analyses carried out in the Upper Red Formation from north and central Iran.

Paleomagnetic Rotations in Central Iran

Paleomagnetic data reveal different amounts of rotation between areas located to the south of the Great Kavir–Doruneh fault (Tabas and Anarak) with respect to areas located in the

Geological Society of America Bulletin, published online on 13 January 2012 as doi:10.1130/B30479.1

TABLE 2. PALEOMAGNETIC ROTATION IN CENTRAL IRAN

Area	Age	Lat, Long (°N, °E)	Pole (λ, ϕ, α_{95})	D, I (exp) (°)	D, I (meas) (°)	R (°) ± Err (°)	F (°) ± Err (°)
Torud*	**Middle–late Miocene**	**35°20′, 54°50′**	**85.0, 155.7, 3.1**	**5.9, 53.5**	**15.2, 41.3**	**9.3 ± 13**	**12.0 ± 10**
Jandaq*	**Middle–late Miocene**	**34°10′, 54°25′**	**85.0, 155.7, 3.1**	**5.9, 52.6**	**6.1, 45.0**	**8.3 ± 15.4**	**8.8 ± 11.1**
Tabas*	**Middle–late Miocene**	**33°30′, 57°00′**	**85.0, 155.7, 3.1**	**5.9, 52.0**	**346.1, 46.1**	**–19.8 ± 8.4**	**5.7 ± 6**
Anarak*	**Eocene–early Miocene**	**33°20′, 53°45′**	**83.8, 153.2, 5.3**	**7.2, 51.3**	**333.2, 29.9**	**–35 ± 18**	**21.4 ± 15.6**
Hadgiabad†	**Eocene**	**33°01′, 59°18′**	**81.3, 162.4, 3.3**	**9.8, 49.8**	**151.1, –30**	**–38.7 ± 6.2**	**19.8 ± 5.5**
She-deh†	**Paleocene**	**33°23′, 59°10′**	**81.1, 190.5, 2.9**	**7.5, 45.7**	**343.3, 59.6**	**–24.2 ± 9.6**	**–13.9 ± 5.5**
Gonabad†	**(Paleocene)**	**34°30′, 58°18′**	**81.1, 190.5, 2.9**	**7.5, 47.1**	**166.2, –54.4**	**–21.3 ± 12.4**	**–7.3 ± 7.5**
Dehuk Sandstones§	**(Aptian–Cenomanian)**	**33°12′, 57°30′**	**81.7, 180.1, 6.7**	**7.9, 47.3**	**326.1, 38.5**	**–41.9 ± 22.1**	**8.8 ± 17.5**
Saghand#	**(Cretaceous)**	**32°30′, 55°12′**	**78.2, 189.4, 2.4**	**9.3, 41.6**	**340.7, 26.3**	**–28.6 ± 3.9**	**15.3 ± 3.8**
Garedu beds§	**(Late Jurassic)**	**34°00′, 56°54′**	**75.0, 159.9, 6.6**	**16.8, 48.5**	**3.9, 41.6**	**–12.8 ± 15.9**	**6.5 ± 12.4**

Note: Paleomagnetic rotation in central Iran from this study (*) and from Bina et al. (1986) (†), Wensink (1982) (§), and Soffel et al. (1996) (#). Abbreviations: Lat, Long—latitude (°N) and longitude (°E) of the sites; pole (λ, ϕ, α_{95})—latitude of the paleopole (°N), longitude of the paleopole (°E), and confidence limit on the paleopole at the 95% level, respectively; D, I (exp)—expected declination and inclination at the site; D, I (meas)—measured declination and inclination at the site; R (°) ± Err (°)—rotation and respective error; F (°) ± Err (°)—flattening and respective error. R and F values (and associated error) were calculated according to the method by Demarest (1983) using the coeval European paleopoles listed in Besse and Courtillot (2002).

Great Kavir Basin to the north of this fault (Torud, Moalleman and Jandaq areas; Fig. 8A). The Anarak and Tabas areas, characterized by the presence of regional NNW-SSE– to N-S–striking right-lateral strike-slip faults, underwent large CCW vertical-axis rotations. In the Torud and Jandaq areas, where ENE-WSW–striking strike-slip and thrust faults prevail, small CW vertical-axis rotations (9.3° ± 13° in the Torud area and 8.3° ± 15° in the Jandaq area) are not statistically different from the coeval expected paleomagnetic direction for central Iran, as the confidence angles are larger than the amount of CW rotations measured in the two localities (see Table 1; Fig. 8A). In the Moalleman structure, a few samples with a primary ChRM reverse polarity show a significant amount of CW rotation, which could also support a possible CW rotation of the blocks located north of the Great Kavir fault. The lack of meaningful clockwise rotations north of the Great Kavir fault, despite structural information, would support the occurrence of such rotations (Allen et al., 2004, 2011; Walker and Jackson, 2004) and needs to be discussed more in detail. One possibility could be that a block-rotation mechanism was active north of the Great Kavir fault and that the different crustal blocks effectively rotated CW during the late Cenozoic together with the left-lateral strike-slip faults, but at a very low rotation rate. In this case, the total amount of CW vertical-axis rotation would be too small to be fully detected with the limited available paleomagnetic data set. A second possibility is that tectonic structures north of the Great Kavir fault (including the eastern Alborz Mountains) have been impacted by different tectonic processes, such as the bend from more linear E-W strike into their current curved geometry, as a consequence of the N-S impingement of central Iran against the eastern Alborz and western Kopeh-Dagh Mountain belts. Such a bending would result in a CCW rotation of crust west of 59°E of longitude, which might have balanced and canceled out the CW rotations associated with left-lateral strike-slip fault activity and block rotations. In the Anarak and Tabas regions, we obtained reliable paleomagnetic results from 5 and 15 sites, respectively. When compared with the coeval Eurasian paleopole, the mean paleomagnetic directions calculated for the two localities show a significant amount of CCW rotations (35° ± 18° for the Anarak area and 19.8° ± 8° for the Tabas area), which are larger than the confidence angles in both localities, showing that both the Tabas and Anarak areas underwent significant CCW rotation during the late Cenozoic.

In central Iran, previous paleomagnetic analyses were carried out in Jurassic to Eocene units from the Tabas, Yazd, and Lut blocks, south of the Great Kavir–Doruneh fault (Wensink, 1982; Bina et al., 1986; Soffel et al., 1996). When compared with the direction expected from the coeval Eurasian paleopoles of Besse and Courtillot (2002), all the study localities show significant CCW rotations. These data are in strong agreement with our results and support the hypothesis that tectonic blocks south of the Great Kavir–Doruneh fault underwent significant CCW vertical-axis rotations during the Cenozoic (Fig. 8A; Table 2).

Accommodation of Shortening in Central Iran

One of the main tectonic implications of our results is that the paleomagnetic data confirm the possibility that some amount of Cenozoic shortening due to Eurasia-Arabia convergence may be accomplished in central Iran by vertical-axis rotation of fault-bounded crustal blocks. Walker and Jackson (2004) calculated the amount of crustal shortening across central Iran that could be accommodated by the CCW rotation of blocks bounded by right-lateral strike-slip faults that are up to ~400 km in length and ~100 km apart. In their scenario, a CCW rotation of 10°–20° (based on structural considerations) would accommodate 7–25 km of N-S shortening. Rotation of blocks bounded by shorter faults would accommodate less shortening. Based on our paleomagnetic results, we calculate shortening considering different lengths of the blocks and using the mean paleomagnetic rotations measured in each area as a measure of vertical-axis rotation of fault-bounded blocks. South of the Great Kavir fault we calculated a N-S shortening of between 25 and 72 km, assuming a block length of 400 km and CCW rotations of 20° and 35° (mean rotation values in the Tabas and Anarak areas; see Table 2), respectively. If we consider shorter blocks (200 km), a N-S shortening of between 12 and 37 km is required to explain 20° and 35° of CCW rotation, respectively (Fig. 8C). North of the Great Kavir fault, the measured CW rotations are not statistically different from the expected coeval paleomagnetic direction for central Iran. However, if we assume a CW rotation of 5.5° to 9.3° (mean rotation values in the Jandaq and Torud areas), and a block length of 100 km (the distance between the Great Kavir and the Torud faults), we should obtain a N-S shortening of 7–12 km (Fig. 8B).

Based on a reconstruction of the Africa-Eurasia plate-motion history, Dewey et al. (1989) calculated an amount of Arabia-Eurasia convergence of ~300–500 km since initial collision at 20–30 Ma. Our data suggest that ~30 to ~80 km (roughly 10%–20% of total shortening) have been accommodated by rotation of right-lateral fault systems. Vertical-axis block rotation is compatible with the deep structure of central Iran, where evidence of shortening by crustal thickening is missing (Hatzfeld and Molnar, 2010).

CONCLUSION

Deformation in Iran has been controlled by the presence of continental blocks (Alborz, Lut, and central Iran), the margins of which

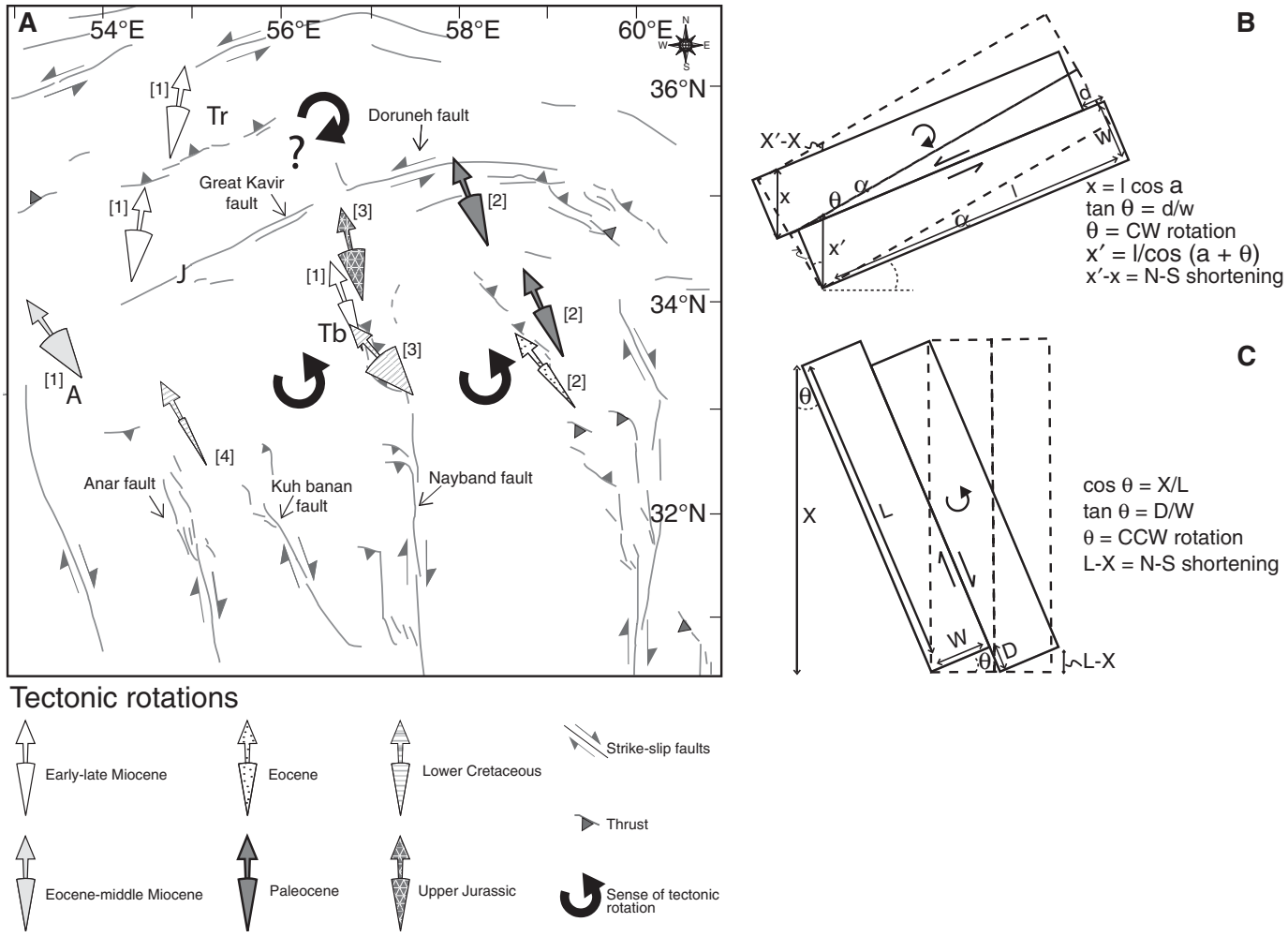

Figure 8. (A) Tectonic rotations from central Iran. Data are from [1] this work; [2] Bina et al. (1986); [3] Wensink (1982); and [4] Soffel et al. (1996). A—Anarak; Tb—Tabas; Tr—Torud; J—Jandaq. Question mark north of the Great Kavir fault indicates that there is no significant support for there having been clockwise rotations in this sector. Cartoon shows how WSW-ENE left-lateral strike-slip faults (B) and NNW-SSE right-lateral (C) in central Iran can accommodate N-S shortening by counterclockwise (CCW) and clockwise (CW) rotation about vertical axes, respectively.

were reactivated during the Cenozoic to accommodate shortening due to Arabia-Eurasia convergence. Paleomagnetic data show that slip on (preexisting) strike-slip faults accommodates vertical-axis rotations of the fault-bounded crustal blocks. North of the Great Kavir fault, where ENE-WSW left-lateral and thrust faults prevail, CW rotations are very small and are not statistically different from the expected paleomagnetic direction for central Iran. Conversely, south of the Great Kavir fault, where N-S right-lateral faults prevail, significant paleomagnetic rotations in the Tabas and Anarak areas were measured. These results confirm previous paleomagnetic data and indicate that the different blocks of central Iran (Tabas, Yazd, and Lut) rotated CCW during the late Cenozoic. Our paleomagnetic data provide the first paleomagnetic constraints to the block-rotation model proposed by Walker and Jackson (2004) and Allen et al. (2004, 2011) to account for late Cenozoic shortening in central Iran, which was based on structural, geomorphologic, and seismic data. Future work will be aimed at evaluating (1) the areal extension and the precise age of the measured paleomagnetic rotations, (2) the possible role of internal deformation within the different blocks, and (3) the role of strain partitioning in accommodating oblique convergence in central Iran. The last two processes are known to have been active in different parts of Iran (Jackson et al., 2002; Zanchi et al., 2006; Walker et al., 2010) and have to be carefully taken into account to usefully relate paleomagnetic rotations to deformation mechanisms.

ACKNOWLEDGMENTS

The authors would like to thank Associate Editor Stephen T. Johnston for accurate and constructive reviews of the manuscript at different stages. James Jackson, Nicholas Swanson-Sysell, and anonymous reviewer are acknowledged for their comments and suggestions, which significantly improved the manuscript. Financial support for this work was provided by MEBE (Middle East Basins Evolution) (proposal 3.30, leader M. Mattei) and DARIUS (proposal: "Paleomagnetic Analyses of Drifting and Tectonic Rotations of Central Iran," leader M. Mattei) programs, in close collaboration with the Geological Survey of Iran.

REFERENCES CITED

Abdalian, S., 1953, Le tremblement de terre de Toroude en Iran: Nature, v. 81, p. 314–319.

Aghanabati, A., 1974, The Geological Map of Tabas: Tehran, Geological Survey of Iran, scale 1:250,000.

Alevi, M., and Houshmand-Zadeh, A., 1976, The Geological Map of Torud: Tehran, Geological Survey of Iran, scale 1:250,000.

Allen, M., Jackson, J., and Walker, R., 2004, Late Cenozoic reorganization of the Arabia-Eurasia collision and the comparison of short-term and long-term deformation rates: Tectonics, v. 23, TC2008, doi:10.1029/2003TC001530.

Allen, M.B., Blanc, E.J., Walker, R., Jackson, J., Talebian, M., and Ghassemi, M.R., 2006, Contrasting styles of convergence in the Arabia-Eurasia collision: Why escape tectonics does not occur in Iran, *in* Dilek, Y., and Pavlides, S., eds., Postcollisional Tectonics and Magmatism in the Mediterranean Region and Asia: Geological Society of America Special Paper 409, p. 579–589, doi:10.1130/2006.2409(26).

Allen, M.B., Kheirkhah, M., Emami, M.H., and Jones, S.J., 2011, Right-lateral shear across Iran and kinematic change in the Arabia–Eurasia collision zone: Geophysical Journal International, v. 184, p. 555–574, doi:10.1111/j.1365-246X.2010.04874.x.

Ambraseys, N., and Moinfar, A., 1977, The Torud earthquake of 12 February 1953: Annali di Geofisica, v. 30, p. 185–200.

Amini, A., 2001, Red coloring of the Upper Red Formation in central part of its basin, Central zone Iran: Journal of Science of Islamic Republic of Iran, v. 12, p. 145–156.

Babakhani, A.R., Susov, M., Dvoryankin, A., Selivanov, E., and Desyaterik, N., 1987, Geological Quadrangle Map of Jandaq: Tehran, Geological Survey of Iran, scale 1:250,000.

Bagheri, S., and Stampfli, G.M., 2008, The Anarak, Jandaq and Posht-e-Badam metamorphic complexes in central Iran: New geological data, relationships and tectonic implications: Tectonophysics, v. 451, p. 123–155, doi:10.1016/j.tecto.2007.11.047.

Ballato, P., Nowaczyk, N.R., Landgraf, A., Strecker, M.R., Friedrich, A., and Tabatabaei, S.H., 2008, Tectonic control on sedimentary facies pattern and sediment accumulation rates in the Miocene foreland basin of the southern Alborz Mountains, northern Iran: Tectonics, v. 27, TC6001, doi:10.1029/2008TC002278.

Berberian, M., 1979a, Earthquake faulting and bedding thrust associated with the Tabas-e-Golshan (Iran) earthquake of September 16, 1978: Bulletin of the Seismological Society of America, v. 69, p. 1861–1887.

Berberian, M., 1979b, Tabas-e-Golshan (Iran) catastrophic earthquake of 16 September 1978; a preliminary field report: Disaster, v. 2, p. 207–219, doi:10.1111/j.1467-7717.1978.tb00099.x.

Berberian, M., 1982, Aftershock tectonics of the 1978 Tabas-e-Golshan (Iran) earthquake sequence: A documented active 'thin- and thick-skinned tectonic' case: Geophysical Journal of the Royal Astronomical Society, v. 68, p. 499–530.

Berberian, M., Asudeh, I., Bilham, R.G., Scholz, C.H., and Soufleris, C., 1979, Mechanism of the main shock and the aftershock study of the Tabas-e-Golshan (Iran) earthquake of September 16, 1978: A preliminary report: Bulletin of the Seismological Society of America, v. 69, p. 1851–1859.

Besse, J., and Courtillot, V., 2002, Apparent and true polar wander and the geometry of the geomagnetic field over the last 200 Myr: Journal of Geophysical Research, v. 107, 2300, doi:10.1029/2000JB000050.

Besse, J., Torcq, F., Gallet, Y., Ricou, L.E., Krystin, L., and Saydi, A., 1998, Late Triassic paleomagnetic data from Iran: Constraints on the migration of the Iranian block through the Tethyan Ocean and initial destruction of Pangea: Geophysical Journal International, v. 135, p. 77–92, doi:10.1046/j.1365-246X.1998.00603.x.

Bina, M., Bucur, I., Prevot, M., Meyerfeld, Y., Daly, L., Cantagrel, J.M., and Mergoil, J., 1986, Palaeomagnetism, petrology and geochronology of Tertiary magmatic and sedimentary units from Iran: Tectonophysics, v. 121, p. 303–329, doi:10.1016/0040-1951(86)90050-8.

Bozorgnia, F., 1966, Qom Formation stratigraphy of the Central Basin of Iran and its intercontinental position: Iranian Petroleum Institute Bulletin, v. 24, p. 69–76.

Demarest, H.H., 1983, Error analysis for the determination of tectonic rotation from paleomagnetic data: Journal of Geophysical Research, v. 88, p. 4321–4328, doi:10.1029/JB088iB05p04321.

Dewey, J.F., Helman, M.L., Turco, E., Hutton, D.H.W., and Knott, S.D., 1989, Kinematics of the western Mediterranean, *in* Coward, M.P., Dietrich, D., and Park, R.G., eds., Alpine Tectonics: Geological Society of London Special Publication 45, p. 265–283.

Eshraghi, S.A., and Jalali, A., 2006, The Geological Map of Moalleman: Tehran, Geological Survey of Iran, scale 1:100,000.

Fisher, R.A., 1953, Dispersion on a sphere: Proceedings of the Royal Society of London, ser. A, v. 217, p. 295–305, doi:10.1098/rspa.1953.0064.

Freund, R., 1970, Rotation of strike slip faults in Sistan, southeast Iran: The Journal of Geology, v. 78, p. 188–200, doi:10.1086/627500.

Gansser, A., 1955, New aspects of the geology of central Iran: Proceedings of the Fourth World Petroleum Congress (Rome, Italy), Section 1/A/5, Paper 2, p. 279–300.

Hatzfeld, D., and Molnar, P., 2010, Comparisons of the kinematics and deep structures of the Zagros and Himalaya and of the Iranian and Tibetan Plateaus and geodynamic implications: Reviews of Geophysics, v. 48, p. 1–48, doi:10.1029/2009RG000304.

Jackson, J., and McKenzie, D.P., 1988, The relationship between plate motion and seismic moment tensors, and the rates of active deformation in the Mediterranean and Middle East: Geophysical Journal of the Royal Astronomical Society, v. 93, p. 45–73.

Jackson, J., and McKenzie, D.P., 1984, Active tectonics of the Alpine-Himalayan belt between western Turkey and Pakistan: Geophysical Journal of the Royal Astronomical Society, v. 77, p. 185–264.

Jackson, J., Haines, J., and Holt, W., 1995, The accommodation of Arabia-Eurasia plate convergence in Iran: Journal of Geophysical Research, v. 100, p. 205–219, doi:10.1029/95JB01294.

Jackson, J., Priestley, K., Allen, M., and Berberian, M., 2002, Active tectonics of the South Caspian Basin: Geophysical Journal International, v. 148, p. 214–245.

Jackson, M.P.A., Cornelius, R., Craig, C., Ganserr, A., Stocklin, J., and Talbot, C., eds., 1990, Salt Diapirs of the Great Kavir, Central Iran: Geological Society of America Memoir 177, 139 p.

Kirschvink, J.L., 1980, The least-squares line and plane and the analysis of paleomagnetic data: Geophysical Journal of the Royal Astronomical Society, v. 62, p. 699–718.

Lowrie, W., 1990, Identification of ferromagnetic minerals in a rock by coercivity and unblocking temperature properties: Geophysical Research Letters, v. 17, p. 159–162, doi:10.1029/GL017i002p00159.

Mattei, M., D'Agostino, N., Zananiri, I., Kondopoulou, D., Pavlides, S., and Spatharas, V., 2004, Tectonic evolution of fault-bounded continental blocks: Comparison of paleomagnetic and GPS data in the Corinth and Megara Basins (Greece): Journal of Geophysical Research, v. 109, p. B02106, doi:10.1029/2003JB002506.

McFadden, P.L., 1990, A new fold test for paleomagnetic studies: Geophysical Journal International, v. 103, p. 163–169, doi:10.1111/j.1365-246X.1990.tb01761.x.

McFadden, P.L., and McElhinny, M.W., 1988, The combined analysis of remagnetization circles and direct observations in paleomagnetism: Earth and Planetary Science Letters, v. 87, p. 161–172, doi:10.1016/0012-821X(88)90072-6.

McFadden, P.L., and McElhinny, M.W., 1990, Classification of the reversal test in palaeomagnetism: Geophysical Journal International, v. 103, p. 725–729, doi:10.1111/j.1365-246X.1990.tb05683.x.

McKenzie, D., and Jackson, J., 1983, The relationship between strain rates, crustal thickening, paleomagnetism, finite strain, and fault movements within a deforming zone: Earth and Planetary Science Letters, v. 65, p. 182–202, doi:10.1016/0012-821X(83)90198-X.

Morley, C.K., Kongwung, B., Julapour, A.A., Abdolghafourian, M., Hajian, M., Waples, D., Warren, J., Otterdoom, H., Srisuriyon, K., and Kazemi, H., 2009, Structural development of a major late Cenozoic basin and transpressional belt in central Iran: The Central Basin in the Qom-Saveh area: Geosphere, v. 5, p. 325–362, doi:10.1130/GES00223.1.

Muttoni, G., Gaetani, M., Kent, D.V., Sciunnach, D., Angiolini, L., Berra, F., Garzanti, E., Mattei, M., and Zanchi, A., 2009a, Opening of the Neo-Tethys Ocean and the Pangea B to Pangea A transformation during the Permian: GeoArabia, v. 14, p. 17–48.

Muttoni, G., Mattei, M., Balini, M., Zanchi, A., Gaetani, M., and Berra, F., 2009b, The drift history of Iran from the Ordovician to the Triassic, *in* Brunet, M.F., Granath, J., and Wilmsen, M., eds., South Caspian to Central Iran Basins: Geological Society of London Special Publication 312, p. 7–29.

Nabavi, M.H., and Houshmand-zadeh, A., 1984, The Geological Map of Anarak: Tehran, Geological Survey of Iran, scale 1:100 000.

Niazi, M., and Kanamori, H., 1981, Source parameters of 1978 Tabas and 1979 Qainat, Iran, earthquakes from long-period surface waves: Bulletin of the Seismological Society of America, v. 71, p. 1201–1213.

Nur, A., and Ron, H., 1987, Kinematics and Mechanics of Tectonic Block Rotation: A Review: U.S. Geological Survey Open-File Report 87–5911, p. 797–823.

Reuter, M., Piller, W.E., Harzhauser, M., Mandic, O., Berning, B., Rogl, F., Kroh, A., Aubry, M.P., Wielandt-Schuster, U., and Hamedani, A., 2009, The Oligo-Miocene Qom Formation (Iran): Evidence for an early Burdigalian restriction of the Tethyan Seaway and closure of its Iranian gateways: International Journal of Earth Sciences, v. 98, p. 627–650, doi:10.1007/s00531-007-0269-9.

Ron, H., Freund, R., and Garfunkel, Z., 1984, Block rotation by strike-slip faulting: Structural and paleomagnetic evidence: Journal of Geophysical Research, v. 89, p. 6256–6270, doi:10.1029/JB089iB07p06256.

Ron, H., Nur, A., and Eyal, Y., 1990, Multiple strike-slip fault sets: A case study from the Dead Sea Transform: Tectonics, v. 9, p. 1421–1431, doi:10.1029/TC009i006p01421.

Sharkovski, M., Susov, M., and Krivyakin, B., 1984, Geology of the Anarak Area (Central Iran). Explanatory Text of the Anarak Quadrangle Map: Tehran, Geological Survey of Iran, scale 1:250,000.

Shirokova, E.T., 1962, Stresses effective in earthquake foci in the Caucasus and adjacent districts: Bulletin of the Russian Academy of Sciences, v. 10, no. 809–815.

Silver, P.G., and Jordan, T.H., 1983, Total-moment earthquakes: Journal of Geophysical Research, v. 88, p. 3273–3293, doi:10.1029/JB088iB04p03273.

Soffel, H.C., Davoudzadeh, M., Rolf, C., and Schmidt, S., 1996, New palaeomagnetic data from central Iran and a Triassic palaeoreconstruction: Geologische Rundschau, v. 85, p. 293–302, doi:10.1007/BF02422235.

Stöcklin, J., and Nabavi, M.H., 1969, Geological Map of Bosurieh: Tehran, Geological Survey of Iran, scale 1:250,000.

Stöcklin, J., and Nabavi, M.H., 1971, Explanatory Text of the Boshruyeh Quadrangle Map, scale 1:250,000: The Geological Survey of Iran, v. J7, p. 1–50.

Stöcklin, J., Eftekhar-Nezhad, J., and Houshmand-Zadeh, A., 1965, Geology of the Shotori Range (Tabas Area East Iran): Geological Survey of Iran Report 3, p. 1–69.

Tchalenko, J.S., 1974, Materials for the study of seismotectonics of Iran; north-central Iran: The Geological Survey of Iran, v. 29, p. 117–216.

Terres, R., and Luyendyk, B., 1985, Neogene tectonic rotation of the San Gabriel region, California, suggested by paleomagnetic vector: Journal of Geophysical Research, v. 90, p. 12,467–12,484, doi:10.1029/JB090iB14p12467.

Vernant, P., Nilforoushan, F., Hatzfeld, D., Abbassi, M.R., Vigny, C., Masson, F., Nankali, H., Martinod, J., Ashtiani, A., Bayer, R., Tavakoli, F., and Chéry, J., 2004, Present-day crustal deformation and plate kinematics in the Middle East constrained by GPS measurements in Iran and northern Oman: Geophysical Journal International, v. 157, p. 381–398, doi:10.1111/j.1365-246X.2004.02222.x.

Walker, R., and Jackson, J., 2004, Active tectonics and late Cenozoic strain distribution in central and eastern Iran: Tectonics, v. 23, p. TC5010, doi:10.1029/2003TC001529.

Walker, R., Jackson, J., and Baker, C., 2003, Surface expression of thrust faulting in eastern Iran: Source parameters and surface deformation of the 1978 Tabas and 1968 Ferdows earthquake sequences: Geophysical Journal International, v. 152, p. 749–765, doi:10.1046/j.1365-246X.2003.01886.x.

Walker, R., Talebian, M., Saiffori, S., Sloan, R., Rasheedi, A., MacBean, N., and Ghassemi, A., 2010, Active faulting, earthquakes, and restraining bend development near Kerman city in southeastern Iran: Journal of Structural Geology, v. 32, p. 1046–1060, doi:10.1016/j.jsg.2010.06.012.

Wells, R., and Hillhouse, J., 1989, Paleomagnetism and tectonic rotation of the lower Miocene Peach Spring Tuff: Colorado Plateau, Arizona to Barstow, California: Geological Society of America Bulletin, v. 101, p. 846–863, doi:10.1130/0016-7606(1989)101<0846:PATROT>2.3.CO;2.

Wensink, H., 1982, Tectonic inferences of paleomagnetic data from some Mesozoic formations in central Iran: Journal of Geophysics, v. 51, p. 12–23.

Zanchi, A., Berra, F., Mattei, M., Ghassemi, M., and Sabouri, J., 2006, Inversion tectonics in central Alborz, Iran: Journal of Structural Geology, v. 28, p. 2023–2037, doi:10.1016/j.jsg.2006.06.020.

Zanchi, A., Zanchetta, S., Garzanti, E., Balini, M., Berra, F., Mattei, M., and Muttoni, G., 2009, The Cimmerian evolution of the Nakhlak-Anarak area, central Iran, and its bearing for the reconstruction of the history of the Eurasian margin, *in* Brunet, M.F., Markus Wilmsen, M., and Granath, J.W., eds., South Caspian to Central Iran Basins: Geological Society of London Special Publication 312, p. 261–286.

Science Editor: Nancy Riggs
Associate Editor: Stephen T. Johnson

Manuscript Received 10 January 2011
Revised Manuscript Received 1 August 2011
Manuscript Accepted 25 August 2011

Printed in the USA